

# Magnetic behavior of $5d^1$ Re-based double perovskite $\text{Sr}_2\text{ZnReO}_6$

Muhammad Maikudi Isah<sup>1</sup>,<sup>1</sup> Biswajit Dalal<sup>2,3</sup>,<sup>2,3</sup> Xun Kang,<sup>2</sup> Dario Fiore Mosca<sup>4</sup>,<sup>4</sup>  
Ifeanyi John Onuorah<sup>5</sup>,<sup>5</sup> Valerio Scagnoli<sup>6,7</sup>,<sup>6,7</sup> Pietro Bonfà<sup>5</sup>,<sup>5</sup> Roberto De Renzi<sup>5</sup>,<sup>5</sup>  
Alexei A. Belik<sup>2</sup>,<sup>2</sup> Cesare Franchini,<sup>4</sup> Kazunari Yamaura<sup>2,8,\*</sup> and Samuele Sanna<sup>1,†</sup>

<sup>1</sup>*Dipartimento di Fisica e Astronomia “A. Righi”, Università di Bologna, I-40127 Bologna, Italy*

<sup>2</sup>*Research Center for Materials Nanoarchitectonics (MANA),*

*National Institute for Materials Science (NIMS), Namiki 1-1, Tsukuba, Ibaraki 305-0044, Japan*

<sup>3</sup>*Department of Physics, Achhruram Memorial College, Jhalda, Purulia, West Bengal, 723202, India*

<sup>4</sup>*University of Vienna, Faculty of Physics and Center for Computational Materials Science, Vienna, Austria*

<sup>5</sup>*Dipartimento di Scienze Matematiche, Fisiche e Informatiche, Università di Parma, I-43124 Parma, Italy*

<sup>6</sup>*Laboratory for Mesoscopic Systems, Department of Materials, ETH Zürich, Zürich, Switzerland*

<sup>7</sup>*PSI Center for Neutron and Muon Sciences, 5232 Villigen PSI, Switzerland*

<sup>8</sup>*Graduate School of Chemical Sciences and Engineering, Hokkaido University,*

*North 10 West 8, Kita-ku, Sapporo, Hokkaido 060-0810, Japan*

(Dated: September 5, 2025)

The subtle interplay between spin-orbit coupling, exchange interactions, and cation ordering can lead to exotic magnetic states in transition-metal ions. We report a comprehensive study of the Re-based ( $5d^1$ ) ordered double perovskite oxide  $\text{Sr}_2\text{ZnReO}_6$  combining synchrotron x-ray diffraction (XRD), magnetic susceptibility, muon spin relaxation ( $\mu\text{SR}$ ) measurements, and density functional theory (DFT) calculations. XRD reveals that  $\text{Sr}_2\text{ZnReO}_6$  crystallizes in the monoclinic structure (space group  $P2_1/n$ ) at low temperature. Magnetic susceptibility data indicate a transition below  $\sim 13$  K, with  $M$ - $H$  loops showing ferromagnetic-like hysteresis and an unusually high coercive field of 23 kOe at 2 K. Zero-field  $\mu\text{SR}$  measurements detect static and spatially disordered internal fields below  $T_M \simeq 12$  K, consistent with a canted antiferromagnetic ground state determined by detailed DFT and force-theorem in Hubbard-I calculations. The reduced high-temperature effective moment ( $\sim 0.76 \mu_B$ ) and very small static moment ( $\leq 0.222 \mu_B$ ) derived from  $\mu\text{SR}$  analysis and local-field simulations indicate a decisive role of spin-orbit coupling. Through a combined experimental and computational approach we unambiguously determine the canted antiferromagnetic order in  $\text{Sr}_2\text{ZnReO}_6$ , showing that a very small ordered moment coexists with an exceptionally large coercivity. These results underscore the crucial role of spin-orbit coupling and orbital ordering, providing new insights into magnetism in  $5d^1$  double perovskites.

## I. INTRODUCTION

The magnetic and orbital ordering in strongly correlated materials plays a crucial role in modern condensed matter physics. In particular, transition-metal ions give rise to a wealth of novel physics properties through the complex interplay of charge, orbital, and spin degrees of freedom [1]. Among the most extensively studied systems are the  $B$ -site ordered double perovskite (DP) oxides, with general formula  $A_2BB'O_6$ , where  $A$  is an alkaline-earth or rare-earth cation and  $B/B'$  are transition-metal ions in different oxidation states. These materials have garnered significant interest owing to the influence of spin-orbit coupling (SOC), electronic correlations and crystal field interactions on the electronic and magnetic properties that drive the emergence of exotic quantum phases [2–4] such as the Mott insulators [5, 6], Weyl semimetals [7–9], half metallicity [10–13] and quantum spin liquids [14].

Generally, the  $B$ -site ordered DPs have been reported to crystallize in the cubic, monoclinic and tetragonal structures and consist of ordered geometry of corner-shared  $BO_6$  and  $B'O_6$  octahedra network, alternatively forming two interpenetrating face-centered (fcc) lattices, and the  $A$  site positioned at the voids between the octahedra [15]. The combination of the  $B$

and  $B'$  sites and the hosting order of the magnetic cations at these sites are crucial determinants of the electronic and magnetic properties, and the nature of the exchange interactions in these compounds. When  $B$  and  $B'$  sites host magnetic ions, the properties are driven by the  $B$ - $O$ - $B'$  mediated super-exchange interaction. However, when magnetic ion resides only on the  $B'$  site, these compounds often become Mott insulators, since the large separation between neighbouring  $B'$  sites reduces the bandwidth and makes the on-site Coulomb repulsion dominant [16]. In such a case, the magnetic interactions are defined by edge-shared network of tetrahedra in a fcc lattice and often exhibit geometric frustration in the presence of antiferromagnetic exchange couplings [17–19]. Further, theoretical studies on analogous DP compounds subjected to strong SOC with only  $B'$  magnetic site hosting either  $4d^n$  or  $5d^n$  electronic state predict the possibility to realize a number of magnetic states including magnetocrystalline anisotropic aligned ferromagnetic (FM) and antiferromagnetic (AFM) states, spin nematic phases, multipolar orders [2, 3, 20] and also canted spin states that are stabilized by Jahn-Teller distortions, owing to the interplay of Heisenberg, non-Heisenberg interactions, and the quadrupolar couplings [21].

In this work, we focus on the Re-based DP  $\text{Sr}_2\text{ZnReO}_6$ , where  $\text{Sr}^{2+}$ , non-magnetic  $\text{Zn}^{2+}$ , and magnetic  $\text{Re}^{6+}$  ( $5d^1$ ) ions occupy the  $A$ ,  $B$  and  $B'$  sites respectively.  $\text{Sr}_2\text{ZnReO}_6$  belongs to a class of materials where experimental measurements revealed a wide variety of structural, magnetic and electronic properties. As mentioned in Ref. [22], these class of materi-

\* yamaura.kazunari@nims.go.jp

† s.sanna@unibo.it

als have no direct correlation between the magnetic ground state and crystal symmetry. For example,  $\text{Ba}_2\text{ZnReO}_6$  exhibits canted ferromagnetic order [23],  $\text{Ba}_2\text{MgReO}_6$  hosts multipolar order [24], and  $\text{Ba}_2\text{YReO}_6$  displays a spin disordered ground state [25], all within the cubic  $Fm\bar{3}m$  structure. The diverse behaviors observed in cubic compounds naturally motivate investigations of tetragonally elongated systems, which have drawn even greater interest due to their unusual magnetic properties. Initially, the isoelectronic compounds  $\text{Sr}_2\text{CaReO}_6$  and  $\text{Sr}_2\text{MgReO}_6$  were suggested to host spin-glass state below  $\approx 14$  K and  $\approx 50$  K, respectively [18, 26], but recently resonant x-ray diffraction experiments on a high-quality  $\text{Sr}_2\text{MgReO}_6$  sample, have proposed a layered antiferromagnetic order at temperatures below  $\approx 55$  K with a propagation vector  $\mathbf{k} = (0, 0, 1)$  [27]. Early theoretical studies predicted that these structures could exhibit antiferromagnetic ordering of magnetic octupoles [28], a phenomenon that has evaded direct experimental confirmation. More recently, theory has pointed to  $\text{Sr}_2\text{MgReO}_6$  as a specific candidate for realizing such ordering [29]. Much less attention has been devoted to understanding the magnetic behavior of  $\text{Sr}_2\text{ZnReO}_6$ , including the role of SOC in stabilizing its ground state. Only the existence of contrasting antiferromagnetic features [15] and weak ferromagnetic transition [30] were detected at low temperature from magnetization measurements, and no magnetic order was detected by neutron diffraction measurements [30]. The unusually small magnetic moment is probably a consequence of strong SOC in  $5d^1$  DPs, combined with effects such as covalency, orbital ordering, and Jahn-Teller distortions, all of which contribute to partial cancellation between spin and orbital magnetism [16].

In this paper, we take advantage of high-quality crystalline samples to revise the crystallographic structure of  $\text{Sr}_2\text{ZnReO}_6$  using synchrotron x-ray diffraction. We then investigate the magnetization dynamics and magnetic structure through bulk magnetization measurements and muon spin rotation and relaxation ( $\mu\text{SR}$ ), the latter being a highly sensitive local probe of magnetism on the atomic scale and ideally suited to detect the very small magnetic moments predicted in this compound. Finally, we complement our experimental findings with DFT+ $\mu$  and force-theorem in Hubbard-I calculations to identify and validate the nature of the magnetic order.

The remainder of this paper is organized as follows; In Sec. II we present both the experimental and computational methods that have been utilized in this work followed by the description of the obtained crystal structure from synchrotron XRD in Sec. III A. In Sec. III B, the magnetization measurements data are presented while the  $\mu\text{SR}$  measurements together with the DFT calculations of the muon sites are presented in Sec. III C and Sec. III C 1, respectively. The identification of the magnetic structure based on force-theorem in Hubbard-I approach and the validation of the structure by the muon local field simulation is presented in Sec. III C 2. The summary is presented in Sec. IV. More details on data analysis are presented in the supplemental material (SM) [31].

## II. EXPERIMENTAL AND COMPUTATIONAL METHODS

Polycrystalline  $\text{Sr}_2\text{ZnReO}_6$  was synthesized via solid-state reaction using SrO (prepared from 99.9% pure  $\text{SrCO}_3$ , Wako Pure Chemical Industries, by heating at  $1300^\circ\text{C}$  in oxygen), ZnO (99.9%, Wako Pure Chemical Industries), and  $\text{ReO}_3$  (synthesized in the lab from 99.99% pure Re, Rare Metallic Co. Ltd.). The powders were mixed in an agate mortar inside an argon-filled glovebox to ensure precise stoichiometry. The mixture was sealed in a platinum capsule and subjected to isotropic compression in a multi-anvil press (CTF-MA1500P, C&T Factory, Tokyo) at 6 GPa and  $1100^\circ\text{C}$  for 1 hour, with an 11-minute ramp to reach the target temperature. After heating, the capsule was rapidly quenched to below  $100^\circ\text{C}$  in 1 minute, followed by slow pressure release over several hours. The resulting product was a dense, polycrystalline black pellet. A portion was ground for phase identification using a Mini-Flex600 x-ray diffractometer (Rigaku, Tokyo) with Cu- $K\alpha$  radiation, and further analyzed by synchrotron XRD with a large Debye-Scherrer camera at BL02B2, SPring-8, Japan [32, 33]. The x-ray wavelength was  $\lambda = 0.65298 \text{ \AA}$ , calibrated using a  $\text{CeO}_2$  standard. Patterns were analyzed and visualized using the RIETAN-VENUS software package [34, 35].

The direct current (dc) magnetic susceptibility ( $\chi$ ) of  $\text{Sr}_2\text{ZnReO}_6$  was measured using a magnetometer (MPMS, Quantum Design, San Diego, CA, USA). The empty sample holder's magnetization was measured to account for its diamagnetic contribution. Measurements were taken from 2–280 K with a 10 kOe magnetic field under both zero-field-cooled (ZFC) and field-cooled (FC) conditions. Isothermal magnetization loops were recorded at various temperatures with the magnetic field swept between  $-70$  kOe and  $+70$  kOe under ZFC conditions. Data reproducibility was confirmed by testing multiple samples from different synthesis runs.

The zero-field (ZF)  $\mu\text{SR}$  measurements were carried out on the GPS spectrometer at the Paul Scherrer Institut (Switzerland) as a function of temperature, ranging from 1.6 K to about 70 K. In a typical ZF- $\mu\text{SR}$  experiment a beam of positive muons 100% spin-polarized along the beam direction is implanted in the sample [36]. The positive muons thermalize at interstitial sites where they act as sensitive probes of development of spontaneous magnetic ordering, precessing in the local magnetic field,  $B_\mu$ , at the Larmor frequency  $\omega_\mu = \gamma_\mu B_\mu$  ( $\gamma_\mu = 2\pi \times 135.5 \text{ MHz/T}$ ). By studying the angular distribution of the positrons emitted during the muon decay process (muon lifetime  $\tau_\mu \approx 2.2\mu\text{s}$ ) we measure the time evolution of the muon-spin asymmetry  $A(t) = A_0 P_z(t)$ , where  $A_0$  is the initial muon asymmetry and  $P_z(t)$  the time dependent muon polarization. The  $\mu\text{SR}$  experimental data were analyzed via least-squares optimization using MUSRFIT software [37] and MULAB, a home-built MATLAB suite.

In order to reliably interpret the  $\mu\text{SR}$  results, it is crucial to accurately determine the muon stopping site, which we have done via DFT calculations within the DFT+ $\mu$  approach [38–41]. A non-spin polarized DFT calculations were carried out using the plane wave (PW) based code Quantum ESPRESSO [42]. The Perdew-Burke-Ernzerhof (PBE) [43] functional was used to estimate the exchange and correlation

term. The muon and the host atoms were modeled with ultra-soft pseudopotentials [44, 45] using 100 Ry and 900 Ry cutoff energy for the wavefunctions and charge density respectively. The muon in the DFT+ $\mu$  procedure was treated as a hydrogen impurity in a charged  $2 \times 2 \times 2$  supercell comprising of 160 host atoms and 1 muon. A  $2 \times 2 \times 2$  Monkhorst-Pack  $k$ -point mesh [46] was used for the Brillouin zone integration. The structural relaxations were carried out until forces and total energy differences were less than 1 mRy/Bohr and 0.1 mRy, respectively. All calculations were performed keeping fixed the experimental lattice parameters (monoclinic phase) reported in Sec. III A below. To resolve the magnetic structure of  $\text{Sr}_2\text{ZnReO}_6$ , additional calculation for local magnetic fields at the muon-stopping sites were performed (see SM [31]).

The magnetic order was determined by calculating the inter-site exchange interactions (IEI) for the general low-energy effective many-body Hamiltonian coupling multipolar moments with total angular momentum  $J_{\text{eff}} = 3/2$  and subject to a monoclinic crystal field (see SM [31]). The calculation involves several steps. To start, the paramagnetic electronic structure of  $\text{Sr}_2\text{ZnReO}_6$  is determined using the charge self-consistent density functional theory with dynamical mean-field theory (DFT+DMFT) [47–50] in the quasi-atomic Hubbard-I (HI) approximation [51]. The DFT calculations were performed using the full-potential LAPW method implemented in Wien2k [52], with the SOC effect included via the standard variational treatment. The local density approximation (LDA) was used for the DFT exchange-correlation potential, together with a 500  $k$ -point mesh in the full Brillouin zone and a basis cutoff of  $R_{\text{mt}}K_{\text{max}} = 7$ . The fully localized limit was adopted for the double-counting correction, assuming the nominal  $5d$  shell occupancy of 1. The Wannier orbitals representing the Re  $d$  states were constructed from the  $d$  Kohn-Sham bands within the energy window  $[-1.36 : 5.44]$  eV relative to the KS Fermi level and the full  $d$ -shell parameters were set to  $F^0 = U = 3.2$  eV and  $J_H = 0.5$  eV, consistent with previous studies on  $d^1$  and  $d^2$  DPs [53–55]. The calculations were performed with fixed (monoclinic) experimental lattice parameters as reported in Sec. III A. Our DFT+HI calculation correctly reproduce the effective atomic level scheme, finding a  $t_{2g} - e_g$  crystal field splitting of  $\sim 4.22$  eV and a SO splitting of  $\sim 0.5$  eV. The  $J_{\text{eff}} = 3/2$  ground state multiplet is further split by the monoclinic crystal field in two doublets separated by  $\sim 0.1$  eV. Since theoretical studies predict that multipolar ordering plays a central role in  $5d^1$  DPs, the multipolar IEI was extracted using the force-theorem in Hubbard-I (FT-HI) approach described in Ref. [56] via the open-source MagInt code [57]. This framework allows the computation of multipolar IEI for general lattice structures with multiple correlated sites and crystal field environments (see SM [31]). All quantities were evaluated in the global reference frame as defined in Fig. 1(b).

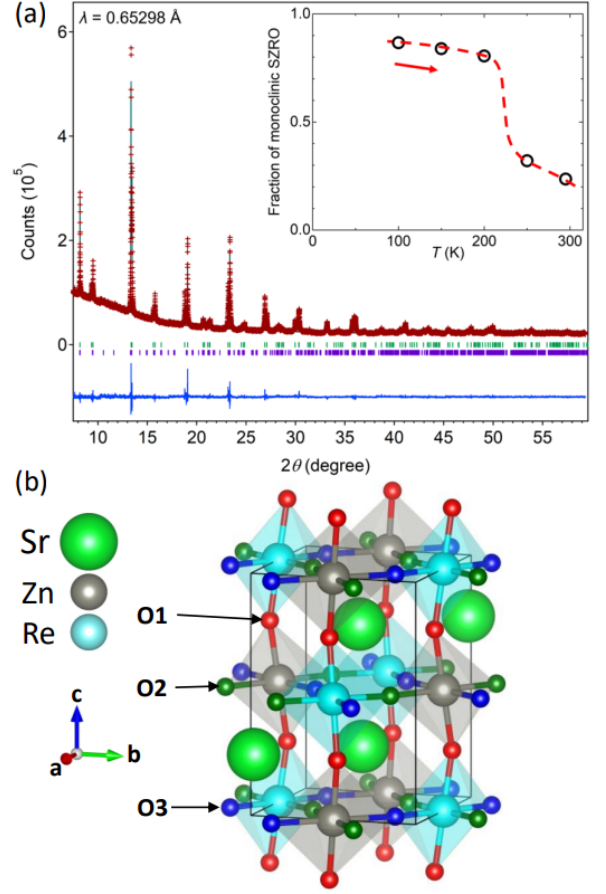


FIG. 1. (a) Synchrotron XRD pattern of  $\text{Sr}_2\text{ZnReO}_6$  at room temperature [298(2) K]. The observed pattern is indicated by red crosses, the calculated pattern by the green solid line, and the difference profile by the blue line. Vertical bars mark the Bragg reflection positions for the tetragonal ( $I4/m$ ; first green ticks) and monoclinic ( $P2_1/n$ ; second violet ticks) models. The inset illustrates the variation in the proportion of the monoclinic phase in the  $\text{Sr}_2\text{ZnReO}_6$  powder with increasing temperature. (b) Crystal structure of monoclinic  $\text{Sr}_2\text{ZnReO}_6$  showing the network of the  $\text{Zn/ReO}_6$  octahedra. The three inequivalent oxygen atoms are represented with spheres of different colors: O1 (red), O2 (green) and O3 (blue).

### III. RESULTS AND DISCUSSION

#### A. Crystal structure

The synchrotron powder x-ray diffraction patterns showed no detectable impurity peaks, indicating that the samples contained only minimal impurities, if any. Previous studies [15, 30] reported a tetragonal phase with the presence of 2.6% to 15% of the monoclinic  $\text{Sr}_2\text{ZnReO}_6$  phase at room temperature, likely due to variations in synthesis conditions. Therefore, we analyzed the diffractograms of the samples across a temperature range of 100 K to 300 K, using a model which takes into account both tetragonal (space group  $I4/m$ ; no. 87) and monoclinic (space group  $P2_1/n$ ; no. 14) phases. As illustrated in Fig. 1(a), the combined analysis of both models



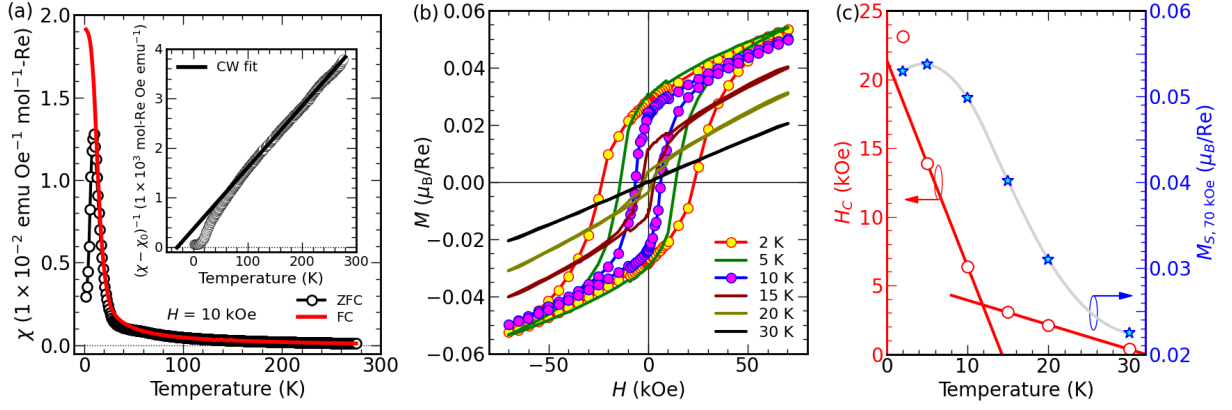


FIG. 2. (a) Temperature dependence of ZFC (open dot) and FC (solid red line) dc magnetic susceptibility ( $\chi(T)$ ; main axes) and inverse of ZFC DC magnetic susceptibility with the CW fit (solid line) ( $(\chi - \chi_0)^{-1}(T)$ ; inset axes) in an applied magnetic field ( $H = 10$  kOe). (b) Isothermal magnetization ( $M$ ) loop as a function of magnetic field ( $H$ ) ranging from -70 to +70 kOe under ZFC mode at six different temperatures. (c) Temperature dependence of coercive field ( $H_c$ ; left axes) and saturation magnetization ( $M_s$ ; right axes) obtained from the ZFC  $M(H)$  loops at  $H = 70$  kOe. The solid lines are guide to the eye unless otherwise stated.

yielded more accurate results than using either model individually. The preliminary analysis of the synchrotron XRD pattern showed no evidence of antisite disorder, which is occasionally observed in DP oxides [58], nor any significant metal or oxygen nonstoichiometry, as previously reported for  $\text{Sr}_2\text{ZnReO}_6$  [15, 30]. Therefore, in the final analysis, the site occupancy of all atoms was fixed as fully occupied. Figure 1(b) shows the crystal structure of the monoclinic phase including the network of corner-shared  $\text{Zn/ReO}_6$  octahedra, while the quantitative details of the lattice parameters and atomic positions of both phases are tabulated in Table S1 in the SM [31].

Having established the structural framework and refined atomic positions, we now turn to the temperature dependence of the crystallographic phases. At 100 K, the monoclinic phase was dominant, comprising 87% of the sample. In contrast, at 300 K, the tetragonal phase became dominant, although 24% of the sample volume is in the monoclinic phase. The phase fraction changed most markedly above 200 K during heating, but the transition remained incomplete even at 300 K. This coexistence of both phases indicates a first-order phase transition, with the transition temperature above 300 K. Our results indicate that this transition is coupled with changes in the degree of tilting and buckling of the bonds between the octahedrally coordinated  $\text{ReO}_6$  and  $\text{ZnO}_6$  units, in agreement with neutron diffraction studies [30]. The thermal evolution of lattice parameters and synchrotron XRD patterns (Fig. S2 of the SM [31]) further supports the occurrence of this first-order structural transition over a broad temperature range.

## B. Magnetic susceptibility and magnetization

Figure 2(a) presents the temperature dependence of the magnetic susceptibility ( $\chi$  vs  $T$ ) in an applied magnetic field of 10 kOe measured on a  $\text{Sr}_2\text{ZnReO}_6$  powder sample between 2 K and 280 K. The ZFC curve shows a peak centered at  $T_p \sim 10$  K; while the FC curve reveals a sharp increase in  $\chi$  at  $T_M \sim 13$

K, implying that the transition at  $T_M$  ( $T_p$ ) has a magnetic origin. This can be further corroborated by the dip in the  $d\chi/dT$  vs  $T$  curve at around 13 K (not shown here). In addition, the frequency independent nature of the ac susceptibility peaks at the transition (see Fig. S3 of the SM [31]) indicates the absence of a glassy magnetic state. The inverse magnetic susceptibility, was fitted [inset to Fig. 2(a)] in the high-temperature range ( $T > 100$  K) by assuming a  $\chi_0$  temperature-independent contribution due to core diamagnetism and Van Vleck paramagnetism, plus a Curie-Weiss (CW) temperature dependence:  $\chi = \chi_0 + C/(T - \Theta_{\text{CW}})$ , where  $C$  is the Curie constant and  $\Theta_{\text{CW}}$  is the CW temperature. The fit yields  $C = 0.072(1)$  emu Oe $^{-1}$  K/mol, and  $\Theta_{\text{CW}} = -20(1)$  K.

The paramagnetic effective moment,  $\mu_{\text{eff}} = \sqrt{8C}\mu_B = 0.758(5) \mu_B/\text{Re}$  is smaller than the calculated value,  $\mu_{\text{cal}} = g\sqrt{S(S+1)}\mu_B = 1.732 \mu_B$ , in the spin only ( $S = 1/2$ ) limit and assuming  $g = 2$ . This discrepancy hints at the likely roles played by the neglected orbital moment and the effects of strong SOC in this compound, as obtainable in several  $5d^1$  DPs. For instance, in the cubic structured  $\text{Ba}_2\text{NaOsO}_6$ , the  $J_{\text{eff}} = 3/2$  quartet ground state has been established and a corrected  $g$ -factor arising from the effect of hybridization with the ligands, has been utilized to compute the paramagnetic effective moment [59]. The extent of the hybridization is represented by a scale factor  $\gamma$ , that reduces the effective orbital momentum from the ideal  $L_{\text{eff}} = -1$  such that  $2S + L_{\text{eff}} \neq 0$  and the  $g$ -factor is  $g = 2(1 - \gamma)/3$ . On this basis, we expect a  $\gamma$  value of 0.41 in comparison to  $\gamma = 0.536$  for  $\text{Ba}_2\text{NaOsO}_6$  [59] and  $\gamma = 0.49$  for  $\text{Ba}_2\text{MgReO}_6$  [60] to explain  $\mu_{\text{eff}} \sim 0.76 \mu_B$  for  $\text{Sr}_2\text{ZnReO}_6$ .

To further elucidate the magnetic behavior of  $\text{Sr}_2\text{ZnReO}_6$ , we recorded isothermal field-dependent magnetization  $M(H)$  curves under ZFC conditions. Figure 2(b) shows the  $M(H)$  curves of  $\text{Sr}_2\text{ZnReO}_6$  at selected temperatures. Notably, magnetization curves at low temperatures ( $T \lesssim 20$  K) display unexpected large hysteresis loops (coercive field  $\sim 23$  kOe at 2 K) indicating the presence of a hard FM-like character with low magnetic moment, whereas at  $T \gtrsim 20$  K, it shows a PM

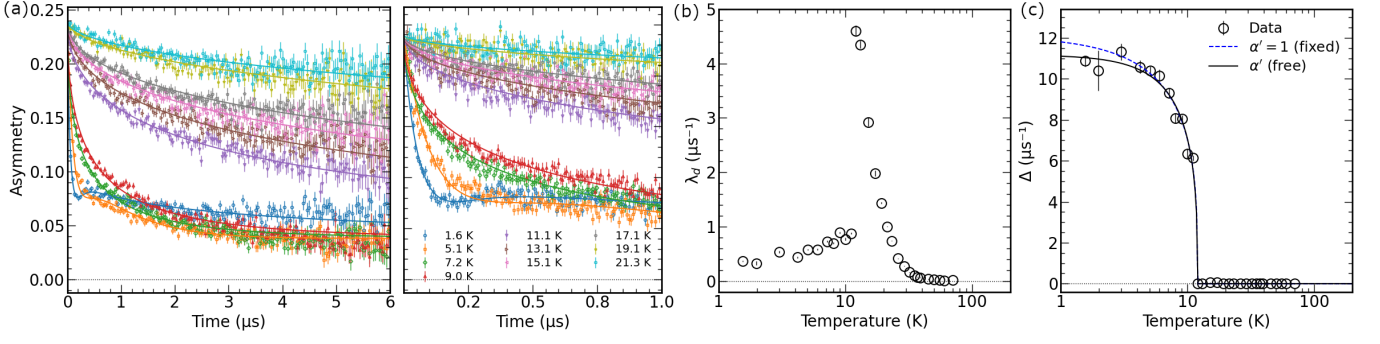


FIG. 3. (a) ZF- $\mu$ SR asymmetry time spectra at different temperatures. The right panel is a zoom for short acquisition time window. Temperature dependence of muon spin relaxation rates (b)  $\lambda_d$  (dynamic), and (c)  $\Delta$  (static) obtained from fit of Eq. (1). The solid and dashed lines are fit to the phenomenological function described in the text.

behavior. The coercive field ( $H_C$ ) is order of magnitude higher than previously reported [30]. On the other hand, the negative sign of  $\Theta_{CW}$  suggests an AFM interaction which appears inconsistent with the observed FM behavior. But then, similar negative  $\Theta_{CW}$  has been measured in ferromagnetic  $\text{Ba}_2\text{MgReO}_6$ ,  $\text{Ba}_2\text{ZnReO}_6$  [22] and  $\text{Ba}_2\text{NaOsO}_6$  [5, 61] compounds, and is attributed to the impact of orbital ordering in the CW behaviour of  $5d^1$  DPs, able to stabilize canted ferromagnetic and noncollinear antiferromagnetic orders [16].

In figure 2(c), we plot temperature dependence of coercive field  $H_C$  (left axes) and saturation magnetization  $M_S$  (right axes). The maximum value obtained for  $H_C$  is 23 kOe at 2 K.  $H_C$  clearly reveals two slopes as a function of temperature. The slope change occurs at about 13 K, corresponding to a coercivity smaller than the value obtained at 2 K by a factor of  $\sim 5$ . As temperature increases, coercivity slowly decreases reaching a minimum value of 0.36 kOe at 30 K. This may suggest that there is no ordered magnetic phase present for temperatures  $T \gtrsim 30$  K. The  $M(H)$  curves remain unsaturated even at 70 kOe as shown in Fig. 2(b), and very small saturated magnetic moment  $\sim 0.05 \mu_B/\text{Re}$  at 2 K is obtained [Fig. 2(c)].

### C. $\mu$ SR

In order to further probe the magnetic behavior of  $\text{Sr}_2\text{ZnReO}_6$ , ZF- $\mu$ SR measurements were performed. The time evolution of muon asymmetry is shown in Fig. 3(a) for temperatures below and above the transition. At all temperatures, the data are best described by the Lorentzian Kubo-Toyabe function multiplied by a stretched-exponential decay function;

$$A(t) = A_1 G_{\text{ZF}}^{\text{Lor}}(\Delta, t) \exp[-(\lambda_d t)^\beta] + A_{\text{bkg}}, \quad (1)$$

where,

$$G_{\text{ZF}}^{\text{Lor}}(\Delta, t) = \frac{1}{3} + \frac{2}{3}[1 - \Delta t] \exp(-\Delta t),$$

and  $A_{\text{bkg}}$  is a constant background term that accounts for muons stopping in the sample holder and cryostat walls.  $G_{\text{ZF}}^{\text{Lor}}$  is

the Kubo-Toyabe (KT) function that describes static relaxation in ZF for a Lorentzian local-field distribution with width  $\Delta/\gamma_\mu$  [62].  $\lambda_d$  is the relaxation rate associated with the dynamic electronic spin fluctuations, and  $\beta$  is the stretched exponent which accounts for distribution of correlation times when  $\beta < 1$  (limited to  $0 < \beta < 1$  for this fit). The function used to fit the data also indicates the presence of a distribution of the magnetic fields at low temperatures and indicates the presence of multiple muon stopping sites in the sample. It is noteworthy to mention that the lack of oscillating component in Eq. (1)—typically observed in materials with long-range magnetic order—suggests the presence of a static but spatially disordered magnetic field. Following, the 1.6 K asymmetry data is well fitted with an exponentially damped oscillating plus relaxing components, which allows to obtain via Fourier transform, the probability distribution density of the muon local field (the fit and Fourier transform are described in Sec. SIII and Fig. S4 of SM [31]).

The temperature dependence of  $\lambda_d$  and  $\Delta$  are shown in Fig. 3(b-c). Figure 3(b) shows that  $\lambda_d$  exhibits a marked critical-like divergence at 12 K ( $\approx T_M$ ).  $\lambda_d$  decreases towards zero for  $T < T_M$  but is still non-vanishing even at the lowest measured temperature of 1.6 K ( $0.36 \mu\text{s}^{-1}$ ), indicating that some fluctuations are still present in the ordered phase. Similar divergence is observed in the temperature dependence of  $\beta$ . The temperature evolution of the static relaxation rate,  $\Delta(T)$  together with the fit curve to a phenomenological order parameter model of the form  $\Delta(T) = \Delta(0)[1 - (T/T_M)^{\alpha'}]^\beta$  is shown in Fig. 3(c). From this fit, we obtain the estimate of the magnetic transition temperature of  $T_{M'} = 12$  K ( $\approx T_M$ ), in agreement with the magnetic susceptibility measurement. The  $\alpha'$  exponent describes the spin wave excitations at low temperatures while  $\beta'$  describes the magnetic interactions and dimensionality of the spin Hamiltonian close to  $T_M$  [63, 64]. To obtain the dashed and solid line in Fig. 3(c),  $\alpha'$  is fixed to 1 and fitted as a free parameter, respectively. The trend as  $T \rightarrow 0$  is not captured with the fixed- $\alpha' = 1$  fit, while the fit with all free parameters yields  $\Delta(0) = 11.2(5) \mu\text{s}^{-1}$ ,  $\alpha' = 1.6(8)$  and  $\beta' = 0.34(8)$ . The  $\alpha'$  value is small (close to the Bloch's  $T^{3/2}$  law) and suggests the presence of ferromagnetic-like order [65], while the  $\beta'$  value is very close to 0.367 expected for

TABLE I. Candidate muon stopping sites in  $\text{Sr}_2\text{ZnReO}_6$  at  $4e$  Wyckoff site symmetries. First and second columns contain the site labels. The positions in fractional coordinates are reported in the third column. The fourth column indicates the energy difference with respect to the lowest energy site  $A_I$ .

Sites	Label	Fractional coord.	$\Delta E$ (meV)
$\mu\text{-O1}$	$A_I$	(0.068, 0.382, 0.792)	0
	$A_{II}$	(0.409, 0.103, 0.707)	106
	$A_{III}$	(0.853, 0.359, 0.806)	118
	$A_{IV}$	(0.213, 0.302, 0.246)	149
$\mu\text{-O2}$	$B_I$	(0.716, 0.806, 0.592)	24
	$B_{II}$	(0.616, 0.698, 0.501)	73
	$B_{III}$	(0.175, 0.043, 0.519)	128
	$B_{IV}$	(0.801, 0.308, 0.151)	175
$\mu\text{-O3}$	$C_I$	(0.804, 0.103, 0.485)	32
	$C_{II}$	(0.713, 0.209, 0.592)	48
	$C_{III}$	(0.164, 0.301, 0.850)	144
	$C_{IV}$	(0.051, 0.170, 0.993)	199

a three-dimensional Heisenberg model of a ferromagnet [66].

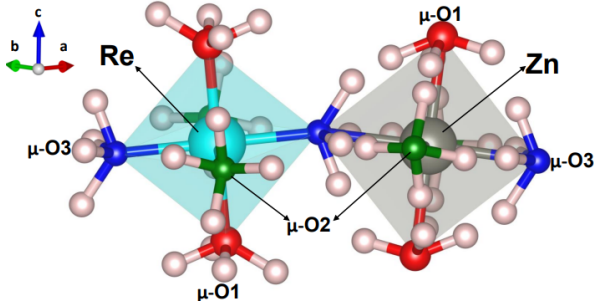


FIG. 4.  $\text{Zn/ReO}_6$  (gray/cyan sphere) octahedra showing the muon stopping sites (pink spheres) bonded to the three distinct oxygen sites (red for O1, green for O2 and blue for O3). The  $\mu\text{-O}_i$  label describes the grouping of inequivalent muons bonded to a distinct O site (see Table I). Plots are reproduced using the VESTA program [34].

### 1. Muon sites

To further analyze the ZF- $\mu\text{SR}$  asymmetry spectra and validate the magnetic structure, the muon-stopping sites in  $\text{Sr}_2\text{ZnReO}_6$  were identified using the standard DFT+ $\mu$  protocol. The results reveal twelve candidate crystal symmetry inequivalent muon positions located in the  $4e$  Wyckoff position in the unit cell. In each case, the muon site forms a bond with an oxygen atom, with a  $\mu\text{-O}$  bond length of  $\approx 1$  Å, as shown in Fig. 4. The positions (Table I) are grouped into  $\mu\text{-O1}$ ,  $\mu\text{-O2}$  and  $\mu\text{-O3}$  sites with respect to the three distinct oxygen. The relative energy differences of all the sites are  $< 0.2$  eV indicating that all candidate sites are most likely occupied even as the zero point motion energy (typically around 0.5 eV [40]) of the muon are not considered. Indeed, the multiple muon sites identified for this compound account for the broad distribution

of the local field in the low temperature  $\mu\text{SR}$  signal, rather than a single field. The form of this distribution includes local fields that vary for the symmetry inequivalent muons closer to each of the three distinct  $\text{O}^{2-}$  ion and equivalent muons closer to either the magnetic  $\text{Re}^{6+}$  ion or the nonmagnetic  $\text{Zn}^{2+}$  ion in the octahedra network.

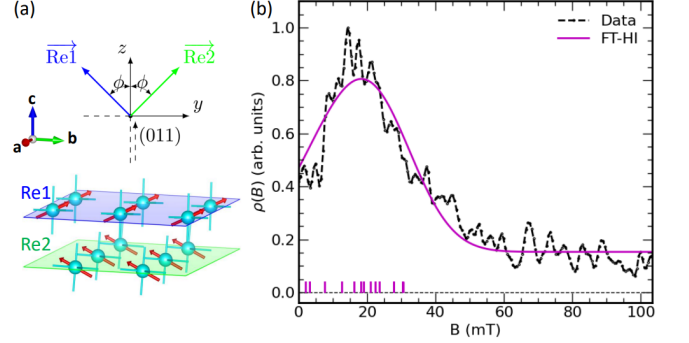


FIG. 5. (a) Schematic illustration of the magnetic configuration showing the canting angle  $\phi$  with spins aligned along (011) plane and the proposed magnetic structure from the FT-HI calculations with canting angle  $\phi = 55^\circ$  between the two magnetic sublattices, labeled Re1 (blue plane) and Re2 (green plane). (b) Comparison between experimental (black line) and fit of the calculated local field distribution  $\rho(B)$  using the proposed magnetic structure (solid magenta colored line). The vertical ticks of same color is the calculated local fields at the muon sites using the magnetic moment obtained from the fit.

### 2. Magnetic structure: FT-HI and muon local field simulations

To identify the ground-state magnetic structure, the low-energy effective Hamiltonian was solved in the presence of monoclinic crystal field within the single site mean-field approximation, relying on the IEI calculated from the FT-HI approach, as described in Sec II. These calculations were achieved using the “McPhase” package [67] together with an in-house module. Due to the quasi-atomic approximation employed, the resulting gyromagnetic factor is  $g_I = 0$  because of the exact compensation of spin and orbital moments, which does not occur in  $\text{Sr}_2\text{ZnReO}_6$ . While covalency effects are implicitly included in the DFT+HI calculation via the Wannier orbitals, calculating the orbital magnetic moment from them is a non trivial procedure [68] and lies beyond the scope of this work. To compute the magnetic moments, we incorporated the covalency effects through the  $\gamma = 1 - 3g_I/2 = 0.41$  factor described previously in Sec. III B. The mean-field result reveal a single second-order phase transition at  $\sim 30$  K towards a canted antiferromagnetic phase with propagation vector  $\mathbf{k} = (0, 0, 1)$  and net magnetic moment of  $\approx 0.04 \mu_B$ , in very good agreement with the magnetization measurements from Fig. 2(b). The overestimation of  $T_N$  (in comparison to 12 K of experiment), well known for mean-field approaches is consistent with the approximation used and with previous studies [54, 55]. In Fig. 5(a), we show the calculated magnetic order including the schematic description of the observed cant-



ing angle  $\phi$  between the two Re sublattices.  $\phi = 0^\circ$  is the FM limit,  $\phi = 90^\circ$  is the AFM limit,  $0^\circ < \phi < 45^\circ$  angles are closer to FM and thus are defined as the canted FM orders, while those within  $45^\circ < \phi < 90^\circ$  correspond to canted AFM orders. The obtained magnetic configuration consists of spin aligned dominantly in the (011) plane and vanishing contribution along x direction, with magnetic moments of magnitude  $\approx 0.06 \mu_B$  and canting angle  $\phi \sim 55^\circ$ . This angle suggests the existence of a canted AFM order.

To validate the calculated magnetic order and the magnitude of the magnetic moment with the ZF- $\mu$ SR asymmetry spectra, we perform local field simulations at the muon-stopping sites [69–72]. The local field for a magnetic configuration is calculated using the expression  $\mathbf{B} \approx \mathbf{B}_{\text{dip}} + \mathbf{B}_{\text{Lor}}$ , where the two terms are the dipole field from the magnetic  $\text{Re}^{6+}$  ions and the Lorentz field respectively [73]. The contact hyperfine contribution arising from the overlap between the muon wavefunction and the magnetic  $\text{Re}^{6+}$  ions is neglected, as vanishing values are expected since the muon positions are relatively far from the magnetic  $\text{Re}^{6+}$ , which also likely host a weak moment. The simulated local field distribution  $\rho(B)$  for the obtained canted AFM order is then fitted to the measured field distribution i.e. the Fourier transform power spectrum in the ZF- $\mu$ SR at  $T = 1.6$  K. The fitting is discussed in more details in the SM [31]. The result is shown in Fig. 5(b), and the simulated field distribution with the proposed canted AFM structure captures the overall features of the experimental data including the peak in the field distribution  $\rho(B)$  with  $R^2 = 0.894$ , signifying the goodness of the fit, validating the obtained magnetic order. A broad distribution of the local field ranging from  $\sim 2$  mT to  $\sim 31$  mT is obtained and assigned to the multiple muon sites. The obtained static magnetic moment from the fit is very small with magnitude of  $0.222(5) \mu_B/\text{Re}$ . Taking into account systematic errors in our analysis and the neglected contact contribution to the local field at the muon sites, a more reliable estimate for the moment at Re is  $\lesssim 0.2 \mu_B$ . This is still larger than the HI estimate, possibly because the hybridization effects are not explicitly taken into account in our calculations, which are known to be strong in this class of materials [74]. As a consequence, it is possible that the effective moment due to hybridization is different and this can affect both DFT+HI estimates as well as DFT+ $\mu$  results through e.g. oxygen polarization.

In all, the obtained canted AFM order is in agreement with the magnetization measurements and reconciles the observed varying FM and AFM signatures in the experimental data. The coexistence of both the large coercive field  $\sim 23$  kOe at 2 K, indicative of FM-like behaviour with low magnetic moment and the negative sign of  $\Theta_{\text{CW}}$  suggesting an AFM interaction is attributed to the impact of orbital ordering in the CW behaviour of  $5d^1$  DPs [16], able to stabilize the obtained canted AFM order.

#### IV. SUMMARY

In summary, we have investigated the crystal structure and magnetic properties of polycrystalline  $\text{Sr}_2\text{ZnReO}_6$ . The crystal structure at room temperature is defined in a tetragonal unit

cell (space group  $I4/m$ ) while at low temperature,  $\text{Sr}_2\text{ZnReO}_6$  undergoes a reduction in symmetry to monoclinic ( $P2_1/n$ ) phase. The magnetic susceptibility data show a sharp increase indicative of a magnetic phase transition below 13 K which is corroborated by ZF- $\mu$ SR measurements where divergence in the temperature dependence of the relaxation rates has been observed at  $T_M \approx 12$  K, below which the existence of static but spatially disordered internal magnetic field, revealed through the presence of multiple muon sites has been measured.  $M$ - $H$  curves indicate an unusually large hysteresis loop with coercive field of 23 kOe at 2 K indicative of a FM-like behavior. On the contrary the fit of the magnetic susceptibility above the magnetic transition show a negative Curie-Wiess constant,  $\Theta_{\text{CW}} = -20$  K indicating AFM correlations.

A canted AFM order was obtained from DFT and force-theorem in Hubbard-I calculations and validated by the simulation of the muon experimental data. The obtained magnetic configuration consists of spin aligned dominantly in the (011) plane and vanishing contribution along x direction, with magnetic moments of magnitude  $\approx 0.06 \mu_B$  and canting angle  $\phi \sim 55^\circ$ . This magnetic order reconciles the hysteretic FM-like behaviour and the AFM character observed with the negative sign of Curie-Wiess temperature.

A small static ordered magnetic moment, of the order of  $0.2 \mu_B/\text{Re}$ , was obtained from the analysis of the muon data, which neglects hybridization effects and can be considered an upper limit. This is further reduced with respect to the paramagnetic effective moment of  $0.76 \mu_B$  obtained from Curie-Wiess fitting of the magnetic susceptibility measurements, and consistent with reduced moment obtainable in  $5d^1$  DPs owing to effect of SOC. To account for the reduced effective moment with respect to the spin only  $1.73 \mu_B$  value, the  $J_{\text{eff}} = 3/2$  quartet-like ground state has been assumed together with covalency effects on the cation orbital moment, underlining the impact of SOC in this compound. These results provide evidence for the magnetic ground state of  $\text{Sr}_2\text{ZnReO}_6$  and guide to the theoretical description of the strong SOC effects envisaged for this and similar compounds.

#### ACKNOWLEDGMENTS

The work here presented is partly supported by project “Spin-charge-lattice coupling in relativistic Mott insulators” (ID No. 202243JHWW, CUP J53D23001350006), funded by European Union–Next Generation EU project–“PNRR–M4C2, investimento 1.1–Fondo PRIN 2022”. This work was also partially supported by a Grant-in-Aid for Scientific Research (No. JP25K01657) from the Japan Society for the Promotion of Science. Synchrotron radiation experiments were conducted at the former NIMS beamline BL15XU of SPring-8 with the permission from the former NIMS synchrotron X-ray station (Proposal Number: 2020A4501). We thank Dr. Y. Katsuya and Dr. M. Tanaka for their help at BL15XU of SPring-8. I. J. O. and R. D. R. acknowledge financial support from the PNRR MUR project ECS-00000033-ECOSISTER. This research was partially granted by University of Parma through the action Bando di Ateneo 2023 per la ricerca. This work is

based on experiments performed at the Swiss Muon Source  $\mu$ S, Paul Scherrer Institute, Villigen, Switzerland. C. F. acknowledges the project “Superlattices of relativistic oxides” (ID No. 2022L28H97) funded by European Union–Next Generation EU project–“PNRR–M4C2, investimento 1.1–Fondo

PRIN 2022”. M. M. I. acknowledges the Computing resources provided by STFC Scientific Computing Department’s SCARF cluster. D. F. M. thanks the computational facilities of the Austrian Scientific Computing (ASC).

- 
- [1] K. I. Kugel’ and D. I. Khomskii, The Jahn-Teller effect and magnetism: transition metal compounds, *Soviet Physics Uspekhi* **25**, 231 (1982).
- [2] G. Chen, R. Pereira, and L. Balents, Exotic phases induced by strong spin-orbit coupling in ordered double perovskites, *Phys. Rev. B* **82**, 174440 (2010).
- [3] W. Witczak-Krempa, G. Chen, Y. B. Kim, and L. Balents, Correlated Quantum Phenomena in the Strong Spin-Orbit Regime, *Annual Review of Condensed Matter Physics* **5**, 57 (2014).
- [4] L. V. Pourovskii, D. Fiore Mosca, L. Celiberti, S. Khmelevskiy, A. Paramekanti, and C. Franchini, Hidden orders in spin–orbit-entangled correlated insulators, *Nature Reviews Materials* **10**, 674 (2025).
- [5] A. S. Erickson, S. Misra, G. J. Miller, R. R. Gupta, Z. Schlesinger, W. A. Harrison, J. M. Kim, and I. R. Fisher, Ferromagnetism in the Mott Insulator  $\text{Ba}_2\text{NaOsO}_6$ , *Phys. Rev. Lett.* **99**, 016404 (2007).
- [6] R. Cong, R. Nanguneri, B. Rubenstein, and V. F. Mitrović, Evidence from first-principles calculations for orbital ordering in  $\text{Ba}_2\text{NaOsO}_6$ : A Mott insulator with strong spin-orbit coupling, *Phys. Rev. B* **100**, 245141 (2019).
- [7] X. Wan, A. M. Turner, A. Vishwanath, and S. Y. Savrasov, Topological semimetal and Fermi-arc surface states in the electronic structure of pyrochlore iridates, *Phys. Rev. B* **83**, 205101 (2011).
- [8] A. A. Burkov and L. Balents, Weyl Semimetal in a Topological Insulator Multilayer, *Phys. Rev. Lett.* **107**, 127205 (2011).
- [9] W. Witczak-Krempa and Y. B. Kim, Topological and magnetic phases of interacting electrons in the pyrochlore iridates, *Phys. Rev. B* **85**, 045124 (2012).
- [10] C. Azimonte, J. C. Cezar, E. Granado, Q. Huang, J. W. Lynn, J. C. P. Campoy, J. Gopalakrishnan, and K. Ramesha, Incipient Orbital Order in Half-Metallic  $\text{Ba}_2\text{FeReO}_6$ , *Phys. Rev. Lett.* **98**, 017204 (2007).
- [11] K.-I. Kobayashi, T. Kimura, Y. Tomioka, H. Sawada, K. Terakura, and Y. Tokura, Intergrain tunneling magnetoresistance in polycrystals of the ordered double perovskite  $\text{Sr}_2\text{FeReO}_6$ , *Phys. Rev. B* **59**, 11159 (1999).
- [12] A. F. García-Flores, A. F. L. Moreira, U. F. Kaneko, F. M. Ardito, H. Terashita, M. T. D. Orlando, J. Gopalakrishnan, K. Ramesha, and E. Granado, Spin-Electron-Phonon Excitation in Re-based Half-Metallic Double Perovskites, *Phys. Rev. Lett.* **108**, 177202 (2012).
- [13] H. Wu, Electronic structure study of double perovskites  $\text{A}_2\text{FeReO}_6$  ( $A = \text{Ba}, \text{Sr}, \text{Ca}$ ) and  $\text{Sr}_2\text{M}\text{MoO}_6$  ( $M = \text{Cr}, \text{Mn}, \text{Fe}, \text{Co}$ ) by LSDA and LSDA +  $U$ , *Phys. Rev. B* **64**, 125126 (2001).
- [14] W. M. H. Natori, M. Daghofer, and R. G. Pereira, Dynamics of a  $j = \frac{3}{2}$  quantum spin liquid, *Phys. Rev. B* **96**, 125109 (2017).
- [15] H. Kato, T. Okuda, Y. Okimoto, Y. Tomioka, K. Oikawa, T. Kamiyama, and Y. Tokura, Structural and electronic properties of the ordered double perovskites  $\text{A}_2\text{MReO}_6$  ( $A = \text{Sr}, \text{Ca}$ ;  $M = \text{Mg}, \text{Sc}, \text{Cr}, \text{Mn}, \text{Fe}, \text{Co}, \text{Ni}, \text{Zn}$ ), *Phys. Rev. B* **69**, 184412 (2004).
- [16] C. Svoboda, W. Zhang, M. Randeria, and N. Trivedi, Orbital order drives magnetic order in  $5d^1$  and  $5d^2$  double perovskite Mott insulators, *Phys. Rev. B* **104**, 024437 (2021).
- [17] A. M. Cook, S. Matern, C. Hickey, A. A. Aczel, and A. Paramekanti, Spin-orbit coupled  $j_{\text{eff}} = 1/2$  iridium moments on the geometrically frustrated fcc lattice, *Phys. Rev. B* **92**, 020417 (2015).
- [18] C. R. Wiebe, J. E. Greedan, G. M. Luke, and J. S. Gardner, Spin-glass behavior in the  $S = 1/2$  fcc ordered perovskite  $\text{Sr}_2\text{CaReO}_6$ , *Phys. Rev. B* **65**, 144413 (2002).
- [19] S. Jana, P. Aich, P. A. Kumar, O. K. Forslund, E. Nocerino, V. Pomjakushin, M. Månsson, Y. Sassa, P. Svedlindh, O. Karis, V. Siruguri, and S. Ray, Revisiting Goodenough-Kanamori rules in a new series of double perovskites  $\text{LaSr}_{1-x}\text{Ca}_x\text{NiReO}_6$ , *Scientific Reports* **9**, 18296 (2019).
- [20] G. Chen and L. Balents, Spin-orbit coupling in  $d^2$  ordered double perovskites, *Phys. Rev. B* **84**, 094420 (2011).
- [21] D. Fiore Mosca, L. V. Pourovskii, B. H. Kim, P. Liu, S. Sanna, F. Boscherrini, S. Khmelevskiy, and C. Franchini, Interplay between multipolar spin interactions, Jahn-Teller effect, and electronic correlation in a  $J_{\text{eff}} = \frac{3}{2}$  insulator, *Phys. Rev. B* **103**, 104401 (2021).
- [22] C. A. Marjerrison, C. M. Thompson, G. Sala, D. D. Maharaj, E. Kermarrec, Y. Cai, A. M. Hallas, M. N. Wilson, T. J. S. Munsie, G. E. Granroth, R. Flacau, J. E. Greedan, B. D. Gaulin, and G. M. Luke, Cubic  $\text{Re}^{6+}$  ( $5d^1$ ) Double Perovskites,  $\text{Ba}_2\text{MgReO}_6$ ,  $\text{Ba}_2\text{ZnReO}_6$ , and  $\text{Ba}_2\text{Y}_{2/3}\text{ReO}_6$ : Magnetism, Heat Capacity,  $\mu\text{SR}$ , and Neutron Scattering Studies and Comparison with Theory, *Inorganic Chemistry* **55**, 10701 (2016).
- [23] V. da Cruz Pinha Barbosa, J. Xiong, P. M. Tran, M. A. McGuire, J. Yan, M. T. Warren, R. V. Aguilar, W. Zhang, M. Randeria, N. Trivedi, D. Haskel, and P. M. Woodward, The Impact of Structural Distortions on the Magnetism of Double Perovskites Containing  $5d^1$  Transition-Metal Ions, *Chemistry of Materials* **34**, 1098 (2022).
- [24] D. Hirai, H. Sagayama, S. Gao, H. Ohsumi, G. Chen, T.-h. Arima, and Z. Hiroi, Detection of multipolar orders in the spin-orbit-coupled  $5d$  Mott insulator  $\text{Ba}_2\text{MgReO}_6$ , *Phys. Rev. Res.* **2**, 022063 (2020).
- [25] C. M. Thompson, J. P. Carlo, R. Flacau, T. Aharen, I. A. Leahy, J. R. Pollicemi, T. J. S. Munsie, T. Medina, G. M. Luke, J. Munevar, S. Cheung, T. Goko, Y. J. Uemura, and J. E. Greedan, Long-range magnetic order in the  $5d^2$  double perovskite  $\text{Ba}_2\text{CaOsO}_6$ : comparison with spin-disordered  $\text{Ba}_2\text{YReO}_6$ , *Journal of Physics: Condensed Matter* **26**, 306003 (2014).
- [26] C. R. Wiebe, J. E. Greedan, P. P. Kyriakou, G. M. Luke, J. S. Gardner, A. Fukaya, I. M. Gat-Malureanu, P. L. Russo, A. T. Savici, and Y. J. Uemura, Frustration-driven spin freezing in the  $S = \frac{1}{2}$  fcc perovskite  $\text{Sr}_2\text{MgReO}_6$ , *Phys. Rev. B* **68**, 134410 (2003).
- [27] S. Gao, D. Hirai, H. Sagayama, H. Ohsumi, Z. Hiroi, and T.-h. Arima, Antiferromagnetic long-range order in the  $5d^1$  double-perovskite  $\text{Sr}_2\text{MgReO}_6$ , *Phys. Rev. B* **101**, 220412 (2020).
- [28] G. Chen, R. Pereira, and L. Balents, Exotic phases induced by



- strong spin-orbit coupling in ordered double perovskites, *Phys. Rev. B* **82**, 174440 (2010).
- [29] D. Fiore Mosca and L. V. Pourovskii, Antiferro octupolar order in the  $5d^1$  double perovskite  $\text{Sr}_2\text{MgReO}_6$  and its spectroscopic signatures, *Phys. Rev. Res.* **7**, L032016 (2025).
- [30] M. Retuerto, M. J. Martínez-Lope, M. García-Hernández, M. T. Fernández-Díaz, and J. A. Alonso, Crystal and Magnetic Structure of  $\text{Sr}_2\text{MReO}_6$  ( $M = \text{Ni, Co, Zn}$ ) Double Perovskites: A Neutron Diffraction Study, *European Journal of Inorganic Chemistry* **2008**, 588 (2008).
- [31] See Supplemental Material at [URL will be inserted by publisher] for FFT spectra and additional data.
- [32] E. Nishibori, M. Takata, K. Kato, M. Sakata, Y. Kubota, S. Aoyagi, Y. Kuroiwa, M. Yamakata, and N. Ikeda, The large Debye–Scherrer camera installed at SPring-8 BL02B2 for charge density studies, *Nuclear Instruments and Methods in Physics Research Section A: Accelerators, Spectrometers, Detectors and Associated Equipment* **467-468**, 1045 (2001), proceedings of the 7th Int. Conf. on Synchrotron Radiation Instrumentation.
- [33] S. Kawaguchi, M. Takemoto, K. Osaka, E. Nishibori, C. Moriyoshi, Y. Kubota, Y. Kuroiwa, and K. Sugimoto, High-throughput powder diffraction measurement system consisting of multiple MYTHEN detectors at beamline BL02B2 of SPring-8, *Review of Scientific Instruments* **88**, 085111 (2017).
- [34] K. Momma and F. Izumi, VESTA: a three-dimensional visualization system for electronic and structural analysis, *Journal of Applied Crystallography* **41**, 653 (2008).
- [35] F. Izumi and K. Momma, Three-Dimensional Visualization in Powder Diffraction, *Solid State Phenomena* **130**, 15 (2007).
- [36] S. J. Blundell, R. De Renzi, T. Lancaster, and F. L. Pratt, *Introduction to Muon Spectroscopy* (Oxford University Press, Oxford, United Kingdom, 2022).
- [37] A. Suter and B. Wojek, Musrfit: A Free Platform-Independent Framework for  $\mu\text{SR}$  Data Analysis, *Physics Procedia* **30**, 69 (2012), 12th International Conference on Muon Spin Rotation, Relaxation and Resonance ( $\mu\text{SR}2011$ ).
- [38] J. S. Möller, P. Bonfà, D. Ceresoli, F. Bernardini, S. J. Blundell, T. Lancaster, R. D. Renzi, N. Marzari, I. Watanabe, S. Sulaiman, and M. I. Mohamed-Ibrahim, Playing quantum hide-and-seek with the muon: localizing muon stopping sites, *Physica Scripta* **88**, 068510 (2013).
- [39] P. Bonfà and R. De Renzi, Toward the Computational Prediction of Muon Sites and Interaction Parameters, *Journal of the Physical Society of Japan* **85**, 091014 (2016).
- [40] S. J. Blundell and T. Lancaster, DFT +  $\mu$ : Density functional theory for muon site determination, *Applied Physics Reviews* **10**, 021316 (2023).
- [41] I. J. Onuorah, M. Bonacci, M. M. Isah, M. Mazzani, R. De Renzi, G. Pizzi, and P. Bonfà, Automated computational workflows for muon spin spectroscopy, *Digital Discovery* **4**, 523 (2025).
- [42] P. Giannozzi, O. Andreussi, T. Brumme, O. Bunau, M. Buongiorno Nardelli, M. Calandra, R. Car, C. Cavazzoni, D. Ceresoli, M. Cococcioni, N. Colonna, I. Carnimeo, A. Dal Corso, S. de Gironcoli, P. Delugas, R. A. DiStasio, A. Ferretti, A. Floris, G. Fratesi, G. Fugallo, R. Gebauer, U. Gerstmann, F. Giustino, T. Gorni, J. Jia, M. Kawamura, H.-Y. Ko, A. Kokalj, E. Küçükbenli, M. Lazzeri, M. Marsili, N. Marzari, F. Mauri, N. L. Nguyen, H.-V. Nguyen, A. Otero-de-la Roza, L. Paulatto, S. Poncé, D. Rocca, R. Sabatini, B. Santra, M. Schlipf, A. P. Seitsonen, A. Smogunov, I. Timrov, T. Thonhauser, P. Umari, N. Vast, X. Wu, and S. Baroni, Advanced capabilities for materials modelling with Quantum ESPRESSO, *Journal of Physics: Condensed Matter* **29**, 465901 (2017).
- [43] J. P. Perdew, K. Burke, and M. Ernzerhof, Generalized Gradient Approximation Made Simple, *Phys. Rev. Lett.* **77**, 3865 (1996).
- [44] D. Vanderbilt, Soft self-consistent pseudopotentials in a generalized eigenvalue formalism, *Phys. Rev. B* **41**, 7892 (1990).
- [45] K. F. Garrity, J. W. Bennett, K. M. Rabe, and D. Vanderbilt, Pseudopotentials for high-throughput DFT calculations, *Computational Materials Science* **81**, 446 (2014).
- [46] H. J. Monkhorst and J. D. Pack, Special points for Brillouin-zone integrations, *Phys. Rev. B* **13**, 5188 (1976).
- [47] A. Georges, G. Kotliar, W. Krauth, and M. J. Rozenberg, Dynamical mean-field theory of strongly correlated fermion systems and the limit of infinite dimensions, *Rev. Mod. Phys.* **68**, 13 (1996).
- [48] V. I. Anisimov, A. I. Poteryaev, M. A. Korotin, A. O. Anokhin, and G. Kotliar, First-principles calculations of the electronic structure and spectra of strongly correlated systems: dynamical mean-field theory, *Journal of Physics: Condensed Matter* **9**, 7359 (1997).
- [49] A. I. Lichtenstein and M. I. Katsnelson, Ab initio calculations of quasiparticle band structure in correlated systems: LDA++ approach, *Phys. Rev. B* **57**, 6884 (1998).
- [50] M. Aichhorn, L. V. Pourovskii, P. Seth, V. Vildosola, M. Zingl, O. E. Peil, X. Deng, J. Mravlje, G. J. Kraberger, C. Martins, *et al.*, TRIQS/DFTTools: A TRIQS application for ab initio calculations of correlated materials, *Computer Physics Communications* **204**, 200 (2016).
- [51] J. Hubbard, Electron correlations in narrow energy bands, *Proc. Roy. Soc. (London)* **A 276**, 238 (1963).
- [52] P. Blaha, K. Schwarz, G. Madsen, D. Kvasnicka, J. Luitz, R. Laskowski, F. Tran, and L. D. Marks, *WIEN2k, An augmented Plane Wave + Local Orbitals Program for Calculating Crystal Properties* (Karlheinz Schwarz, Techn. Universität Wien, Austria, ISBN 3-9501031-1-2, 2018).
- [53] D. Fiore Mosca, L. V. Pourovskii, B. H. Kim, P. Liu, S. Sanna, F. Boscherini, S. Khmelevskiy, and C. Franchini, Interplay between multipolar spin interactions, Jahn-Teller effect, and electronic correlation in a  $J_{\text{eff}} = \frac{3}{2}$  insulator, *Phys. Rev. B* **103**, 104401 (2021).
- [54] D. Fiore Mosca, C. Franchini, and L. V. Pourovskii, Interplay of superexchange and vibronic effects in the hidden order of  $\text{Ba}_2\text{MgReO}_6$  from first principles, *Phys. Rev. B* **110**, L201101 (2024).
- [55] L. V. Pourovskii, D. Fiore Mosca, and C. Franchini, Ferrooctupolar Order and Low-Energy Excitations in  $d^2$  Double Perovskites of Osmium, *Phys. Rev. Lett.* **127**, 237201 (2021).
- [56] L. V. Pourovskii, Two-site fluctuations and multipolar intersite exchange interactions in strongly correlated systems, *Phys. Rev. B* **94**, 115117 (2016).
- [57] L. V. Pourovskii and D. Fiore Mosca, MagInt, <https://github.com/MagInteract/MagInt>.
- [58] R. C. Sahoo, Y. Takeuchi, A. Ohtomo, and Z. Hossain, Exchange bias and spin glass states driven by antisite disorder in the double perovskite compound  $\text{LaSrCoFeO}_6$ , *Phys. Rev. B* **100**, 214436 (2019).
- [59] K.-H. Ahn, K. Pajskr, K.-W. Lee, and J. Kuneš, Calculated  $g$ -factors of  $5d$  double perovskites  $\text{Ba}_2\text{NaOsO}_6$  and  $\text{Ba}_2\text{YOsO}_6$ , *Phys. Rev. B* **95**, 064416 (2017).
- [60] D. Hirai and Z. Hiroi, Successive Symmetry Breaking in a  $J_{\text{eff}} = 3/2$  Quartet in the Spin–Orbit Coupled Insulator  $\text{Ba}_2\text{MgReO}_6$ , *Journal of the Physical Society of Japan* **88**, 064712 (2019).
- [61] R. Cong, E. Garcia, P. C. Forino, A. Tassetti, G. Allodi, A. P. Reyes, P. M. Tran, P. M. Woodward, C. Franchini, S. Sanna, and V. F. Mitrović, Effects of charge doping on Mott insulator with strong spin-orbit coupling,  $\text{Ba}_2\text{Na}_{1-x}\text{Ca}_x\text{OsO}_6$ , *Phys. Rev. Mater.* **7**, 084409 (2023).

- [62] Y. J. Uemura, T. Yamazaki, D. R. Harshman, M. Senba, and E. J. Ansaldo, Muon-spin relaxation in AuFe and CuMn spin glasses, *Phys. Rev. B* **31**, 546 (1985).
- [63] P. J. Baker, T. Lancaster, I. Franke, W. Hayes, S. J. Blundell, F. L. Pratt, P. Jain, Z.-M. Wang, and M. Kurmoo, Muon spin relaxation investigation of magnetic ordering in the hybrid organic-inorganic perovskites  $[(\text{CH}_3)_2\text{NH}_2]M(\text{HCOO})_3$  ( $M = \text{Ni}, \text{Co}, \text{Mn}, \text{Cu}$ ), *Phys. Rev. B* **82**, 012407 (2010).
- [64] R. Peřka, P. Konieczny, M. Fitta, M. Czapla, P. M. Zieliński, M. Bałanda, T. Wasiutyński, Y. Miyazaki, A. Inaba, D. Pinkowicz, and B. Sieklucka, Magnetic systems at criticality: Different signatures of scaling, *Acta Physica Polonica A* **124**, 977 (2013).
- [65] S. Blundell, *Magnetism in Condensed Matter* (Oxford University Press, Oxford, United Kingdom, 2001).
- [66] M. F. Collins, *Magnetic Critical Scattering* (Oxford University Press, New York, 1989) p. 29.
- [67] M. Rotter, Using McPhase to calculate magnetic phase diagrams of rare earth compounds, *Journal of Magnetism and Magnetic Materials* **272-276**, E481 (2004), proceedings of the International Conference on Magnetism (ICM 2003).
- [68] K.-H. Ahn, K. Pajskr, K.-W. Lee, and J. Kuneš, Calculated  $g$ -factors of  $5d$  double perovskites  $\text{Ba}_2\text{NaOsO}_6$  and  $\text{Ba}_2\text{YOsO}_6$ , *Phys. Rev. B* **95**, 064416 (2017).
- [69] A. J. Steele, P. J. Baker, T. Lancaster, F. L. Pratt, I. Franke, S. Ghannadzadeh, P. A. Goddard, W. Hayes, D. Prabhakaran, and S. J. Blundell, Low-moment magnetism in the double perovskites  $\text{Ba}_2\text{MOsO}_6$  ( $M = \text{Li}, \text{Na}$ ), *Phys. Rev. B* **84**, 144416 (2011).
- [70] P. Bonfà, M. M. Isah, B. A. Frandsen, E. J. Gibson, E. Brück, I. J. Onuorah, R. De Renzi, and G. Allodi, Ab initio modeling and experimental investigation of  $\text{Fe}_2\text{P}$  by DFT and spin spectroscopies, *Phys. Rev. Mater.* **5**, 044411 (2021).
- [71] I. J. Onuorah, J. Frassinetti, Q. Wang, M. M. Isah, P. Bonfà, J. G. Rau, J. A. Rodriguez-Rivera, A. I. Kolesnikov, V. F. Mitrović, S. Sanna, and K. W. Plumb, Unraveling the magnetic ground state in the alkali-metal lanthanide oxide  $\text{Na}_2\text{PrO}_3$ , *Phys. Rev. B* **110**, 064425 (2024).
- [72] M. Sahoo, I. J. Onuorah, L. C. Folkers, E. Kochetkova, E. V. Chulkov, M. M. Otrokov, Z. S. Aliev, I. R. Amiraslanov, A. U. B. Wolter, B. Büchner, L. T. Corredor, C. Wang, Z. Salman, A. Isaeva, R. De Renzi, and G. Allodi, Ubiquitous Order-Disorder Transition in the Mn Antisite Sublattice of the  $(\text{MnBi}_2\text{Te}_4)(\text{Bi}_2\text{Te}_3)_n$  Magnetic Topological Insulators, *Advanced Science* **11**, 2402753 (2024).
- [73] P. Bonfà, I. J. Onuorah, and R. D. Renzi, Introduction and a Quick Look at MUESR, the Magnetic Structure and mUon Embedding Site Refinement Suite, in *Proceedings of the 14th International Conference on Muon Spin Rotation, Relaxation and Resonance ( $\mu\text{SR}2017$ )*, Vol. 21 (2018).
- [74] S. Agrestini, F. Borgatti, P. Florio, J. Frassinetti, D. Fiore Mosca, Q. Faure, B. Detlefs, C. J. Sahle, S. Francoual, J. Choi, M. Garcia-Fernandez, K.-J. Zhou, V. F. Mitrović, P. M. Woodward, G. Ghiringhelli, C. Franchini, F. Boscherini, S. Sanna, and M. Moretti Sala, Origin of Magnetism in a Supposedly Nonmagnetic Osmium Oxide, *Phys. Rev. Lett.* **133**, 066501 (2024).